

1 ***Revision 1***

2
3 **Static compression of B2 KCl to 230 GPa and its *P-V-T* equation of**
4 **state**

5
6 **SHIGEHIKO TATENO^{1,*}, TETSUYA KOMABAYASHI², KEI HIROSE^{1,3},**
7 **NAOHISA HIRAO⁴, AND YASUO OHISHI⁴**
8

9 ¹Earth-Life Science Institute, Tokyo Institute of Technology, 2-12-1 Ookayama, Meguro, Tokyo
10 152-8550, Japan

11 ²School of GeoSciences and Centre for Science at Extreme Conditions, University of Edinburgh,
12 Grant Institute, The King's Buildings, James Hutton Road, Edinburgh EH9 3FE, U.K.

13 ³Department of Earth and Planetary Science, The University of Tokyo, 7-3-1 Hongo, Bunkyo,
14 Tokyo 113-0033, Japan

15 ⁴Japan Synchrotron Radiation Research Institute, 1-1-1 Kouto, Sayo-cho, Hyogo 679-5198, Japan
16

17 **ABSTRACT**

18 The pressure-volume-temperature (*P-V-T*) measurements of the B2 (CsCl-type)
19 phase of KCl were performed at 9–61 GPa / 1500–2600 K and up to 229 GPa at room
20 temperature, based on synchrotron X-ray diffraction measurements in a laser-heated
21 diamond-anvil cell (DAC). The nonhydrostatic stress conditions inside the sample
22 chamber were critically evaluated based on the platinum pressure marker. With thermal
23 annealing by laser after each pressure increment, the deviatoric stress was reduced to less
24 than 1% of the sample pressure even at the multi-Mbar pressure range. The obtained *P-V-*
25 *T* data were fitted to the Vinet equation of state with the Mie-Grüneisen-Debye model for
26 thermal pressure. The Grüneisen parameter at ambient condition was found to be as small
27 as 0.58(±0.05), which represents a small thermal pressure. Such a low thermal pressure
28 validates the use of a KCl pressure medium as a pressure marker at high temperatures.

29 **Key words:** KCl, equation of state, high pressure, DAC
30 -----

31 * E-mail: tateno@elsi.jp (S. Tateno)

32

33

INTRODUCTION

34 Potassium chloride is often used as a pressure gauge and pressure-transmitting
35 medium in high-pressure experiments using a DAC because it hardly reacts with silicates
36 and metals and provides lesser deviatoric stress inside the sample chamber. Moreover, it
37 can be used for very high temperature experiments such as melting experiments (e.g.,
38 Anzellini et al. 2013; Andrault et al. 2014; Morard et al. 2017), since the melting
39 temperature of KCl is much higher than that of NaCl (Boehler et al. 1997). KCl is also
40 useful for synchrotron-based experiments when the X-ray beam is accurately aligned to a
41 heating laser beam spot as X-ray induces visible fluorescent light in KCl in a wide
42 pressure range, although the diffraction peaks are stronger compared to NaCl.

43 The B1-phase of KCl with the NaCl-type structure transforms into the B2 (CsCl-
44 type) structure at 2 GPa (Walker et al. 2002). Equations of state (EoS) of B2 KCl have
45 been proposed from experimental studies in a multi-anvil press or DAC (Yagi 1978;
46 Campbell and Heinz 1991; Walker et al. 2002; Dewaele et al. 2012). Cold compression
47 experiments on KCl in a helium pressure medium performed up to 160 GPa reported its
48 highly compressible nature comparable to solid argon (Dewaele et al. 2012). Walker et al.
49 (2002) reported that B2 KCl exhibits low thermal expansivity up to 8 GPa and 873 K,
50 which was supported by recent theoretical calculations by Dewaele et al. (2012). The low
51 thermal expansivity may provide the opportunity for KCl to serve as a practical pressure
52 standard at high temperature even when it is used as a pressure medium; namely, a large
53 temperature gradient, if any, across the pressure medium may not matter when calculating
54 the sample pressure from its P - V - T EoS. Hence, precise evaluation of its thermal EoS is

55 of great importance for high P - T experiments in the DAC. Here we present a new EoS for
56 B2-type KCl from our high P - T experiments to 230 GPa/300K and 60 GPa/2600 K in a
57 laser-heated DAC.

58

59

EXPERIMENTAL METHODS

60 High P - T conditions were generated using laser-heated DAC techniques. Diamond–
61 anvils with a culet size of 300, 120, or 40 μm were used depending on the target pressure.
62 The starting material was powder of KCl (Wako Pure Chemical Industries, Ltd., 99.5%
63 purity) which was mixed with platinum black that served as an internal pressure standard
64 and laser absorber. The sample mixture was loaded into a hole drilled in a Re-gasket
65 together with insulation layers. We used SiO_2 glass (runs #1 and #2) or argon (runs #5
66 and #6) for thermal insulation. Argon was cryogenically loaded into the sample chamber.
67 The sample assembly was then dried by leaving the cell in a vacuum oven at 393 K for
68 >1 h prior to pressurizing, and flushed with argon gas when the oven was opened. The
69 sample pressure was calculated from the unit-cell volume of Pt based on the EoS
70 proposed by Sokolova et al. (2016).

71 Angle-dispersive XRD measurements were conducted at BL10XU, SPring-8 (Ohishi
72 et al. 2008). XRD patterns were collected on an imaging plate (*Rigaku R-AXIS IV*). The
73 typical exposure time was 2 min. Monochromatic incident X-rays were focused by
74 stacked compound refractive lenses and collimated to an area of approximately 6- μm
75 full-width at half maximum (FWHM) at the sample position. The wavelength was
76 precisely determined during each beamtime using a CeO_2 standard: 0.4133–0.4135 \AA
77 (~ 30 keV). Two-dimensional XRD images were integrated over the Debye–Scherrer

78 rings using the IPAnalyzer program (Seto et al. 2010) in order to produce conventional
79 one-dimensional diffraction patterns as a function of two-theta angle. The obtained peak
80 profiles and backgrounds were fit to pseudo-Voigt line shapes within the software
81 package of PDindexer (Seto et al. 2010). The lattice parameters were obtained by a least-
82 squares fit of peak positions. The unit-cell volumes were determined by averaging lattice
83 parameters from 3–6 peaks and 2–5 peaks for Pt and B2 KCl, respectively after careful
84 selection based on stress analysis (see below). Weak or poorly resolved diffraction peaks
85 were not used in volume determination or stress analysis. Heating was performed from
86 both sides of the sample by employing a pair of 100 W single-mode Yb fiber lasers (*SPI*).
87 Temperatures were measured by a spectroradiometric method (Ohishi et al. 2008). In
88 order to reduce the radial temperature gradient, we used beam shapers (*New focus*) that
89 convert a beam with a Gaussian intensity distribution to one with a flat-top distribution.
90 The sample temperatures reported in this study are the average in the 6- μm region probed
91 by X-rays around the hot spot.

92

93 **RESULTS AND DISCUSSION**

94 Four separate sets of experiments were performed to measure the unit-cell volume
95 of B2 KCl and Pt at 84.8–229 GPa at 300 K (runs #1 and 2) and 4.2–59.4 GPa at 300–
96 2560 K (runs #3 and 4). The observed unit-cell parameters and volumes are summarized
97 in Table 1. Representative XRD patterns are shown in Fig. 1, in which diffraction peaks
98 from B2 KCl, Pt, and Ar pressure medium were found. Diffraction peaks from SiO₂ were
99 not observed through the present experiments; crystallization of SiO₂ glass is known to be
100 quite sluggish (Komabayashi et al. 2012; Tateno et al. 2015). We employed laser heating

101 in order to reduce potential deviatoric stress in the sample as well as to measure the
102 sample volume at high temperatures. The laser beam was carefully rastered over the
103 whole sample at 1300–4000 K for 5–10 min depending on the pressure. We measured the
104 unit-cell volume at 300 K after thermal annealing. The diffraction peaks from B2 KCl
105 and Pt became sharp due to heating and spotty reflections also appeared on the diffraction
106 rings. The following compression at room temperature significantly broadened the peaks
107 and some of the diffraction spots disappeared, particularly for B2 KCl (Supplemental Fig.
108 S1). This is likely due to reduction in the grain size and/or increase of micro-stresses as
109 discussed below. Subsequently, the sharp and spotty diffractions were again observed on
110 laser heating. The grain growth of B2 KCl was confirmed up to 250 GPa and 3500 K,
111 suggesting its thermodynamic stability.

112 **Nonhydrostaticity**

113 Potential sources for the systematic errors in the unit-cell volume measurement
114 include the presence of nonhydrostatic stress conditions induced by uniaxial compression
115 in the DAC. Here we evaluated the nonhydrostatic stress conditions inside the sample
116 chamber from diffraction line shifts and peak widths before/after heating. Uniaxial
117 compression develops the differential stress, t , defined as the difference between the
118 maximum stress along the compression axis and the minimum stress in the radial
119 direction. The differential stress results in variation in the lattice parameter as a function
120 of crystallographic orientation (hkl). Sing and Takemura (2001) proposed a linear relation
121 between the measured lattice parameter for a given hkl , $a_m(hkl)$, and $3(1-3\sin^2\theta)\Gamma(hkl)$,
122 referred to as the gamma plot, where θ is the diffraction angle and $\Gamma(hkl) = (h^2k^2 + k^2l^2 +$
123 $l^2h^2)/(h^2 + k^2 + l^2)^2$. The St value can be derived directly from the intercept (M_0) and slope

124 (M_1) of the gamma plot: $St = -3M_1/M_0$, where S is the single-crystal elastic compliance.
125 The differential stress in platinum can be calculated with the pressure dependence of the
126 S value from the theoretical study (Menéndez -Proupin and Singh 2007). On the other
127 hand, since S of B2 KCl is not available under pressure, we examined the St value for B2
128 KCl as a stress indicator. The gamma plots for Pt and KCl at selected pressures are shown
129 in Figure 2. The slope was significantly reduced by laser annealing for both materials.
130 The differential stress measured in Pt at 229 GPa, the highest pressure achieved in this
131 study, was as small as 0.7 GPa after annealing. The t values observed after heating in this
132 study were up to 1% of the pressure. These are much lower than the t values measured in
133 the cold compression using a He pressure medium (Dorfman et al. 2012). Similarly, the
134 laser heating decreased the magnitude of the St value of KCl. $|St|$ obtained to 100 GPa
135 typically ranged from 0 to 0.005, and increased to 0.012 at 229 GPa. In particular, the
136 lattice parameters calculated from each of the (200) and (400) lines of Pt are largely
137 deviated, implying that these reflections are most affected by uniaxial compression. This
138 observation is commonly observed in previous experimental studies on cubic phases such
139 as platinum, gold, and CaSiO_3 perovskite (Shim et al. 2000; Takemura and Dewaele
140 2008; Sakai et al. 2011; Dorfman et al. 2012). Similarly, the gamma plots for B2 KCl
141 indicate that the effect of the uniaxial stress is largest for $a_m(200)$. Figure 3 shows the
142 variation of the t and St values of Pt and KCl, respectively, which were measured
143 before/after laser hearing. The deviatoric stress always developed upon compression at
144 room temperature, leading to scattered data points. Subsequent laser heating clearly made
145 the stress smaller, although greater compressions >100 GPa showed larger deviatoric
146 stresses even after laser annealing. In summary, (i)the thermal annealing made in our

147 experiments reduced the deviatoric stress and (ii) the use of the (200) and (400) lines of Pt
148 and the (200) line of B2 KCl introduces systematic errors in the calculated unit-cell
149 volumes. The selection of the diffraction lines based on the gamma plot can minimize the
150 nonhydrostatic effect on volume determination (Takemura and Dewaele 2008; Dewaele
151 et al. 2012). Due to (ii), we did not use the (200) and (400) lines of Pt and the (200) line
152 of B2 KCl.

153 The width of a powder diffraction line (hkl) is related to the micro-stresses in a
154 powder material (inter-grain stress) and grain size (e.g., Sing et al. 2008). Figure 4 shows
155 the FWHM of the most intense reflections of (111) line and (110) line from Pt and KCl,
156 respectively, normalized to the diffraction angle 2θ as a function of pressure. The FWHM
157 of both Pt and KCl significantly decreased upon laser heating, suggesting grain growth or
158 reduced micro-stress which is at a similar level to that observed in the CeO₂ standard
159 comparable to instrumental resolution. We note that laser heating is very useful to reduce
160 macro/micro stresses in the sample (e.g., Uts et al. 2013). The FWHM observed at 6–18
161 GPa was anomalously large even after heating, although the measured deviatoric stresses
162 indicates quasi-hydrostatic conditions (Fig. 3a). This observation suggests the micro-
163 stress resulting from grain contact is relatively large under such small compression, even
164 if the aggregate itself is hydrostatically compressed. The systematic increase of FWHM
165 on compression is likely caused by a combined effect of the decreased grain size and
166 increased micro-stress.

167 As mentioned above, we made efforts to minimize the effects of the deviatoric
168 stress by employing thermal annealing and choosing the diffraction lines for calculating
169 the unit-cell volume. As a result, our P – V – T data in Table 1 represent much lesser

170 nonhydrostatic conditions than in the case of a He pressure medium without thermal
171 annealing (Figs. 3 and 4).

172 **Equation of state at room temperature**

173 We collected unit-cell volume data at 300 K up to 229 GPa, all after thermal
174 annealing. The measured P – V data were fitted to the Vinet EoS (Fig. 5a):

$$175 \quad P(V, T_0) = 3K_0 \left(\frac{V}{V_0}\right)^{-2/3} \left[1 - \left(\frac{V}{V_0}\right)^{1/3}\right] \exp\left\{\frac{3}{2}(K'_0 - 1) \left[1 - \left(\frac{V}{V_0}\right)^{1/3}\right]\right\} \quad (1)$$

176 where V_0 , K_0 , and K'_0 are the unit-cell volume, isothermal bulk modulus, and its pressure
177 derivative at the reference P – T condition that is 1 bar and 300 K. In the fitting procedure,
178 due to the lack of sufficient data at low pressure near ambient condition in this study, we
179 fixed V_0 at 54.5 \AA^3 from the literature (Dewaele et al. 2012) which was precisely
180 constrained under hydrostatic condition below 10 GPa with a single crystal KCl loaded in
181 liquid He. We then fitted all the remaining parameters simultaneously, including
182 thermoelastic parameters mentioned below. The fitting yielded K_0 and K'_0 to be $18.3 \pm$
183 0.3 GPa and 5.60 ± 0.03 , respectively, based on the Pt pressure scale by Sokolova et al.
184 (2016). Another fitting based on Holmes et al. (1989)'s Pt scale leads to similar values of
185 $K_0 = 17.4 \pm 0.2 \text{ GPa}$ and $K'_0 = 5.76 \pm 0.03$. The fitting results are summarized in Table 2.
186 Our compression curve is in good agreement with the recent results by Dewaele et al.
187 (2012) to $\sim 50 \text{ GPa}$, above which the two curves however deviate from each other slightly
188 (Fig. 5a). Figure 6a compares the calculated pressure between the previous EoS reported
189 by Dewaele et al. (2012) and ours with calibration against various Pt scales (Holmes et al.
190 1989; Dorogokupets and Oganov 2007; Yokoo et al. 2009; Ono et al. 2010; Dorfman et al.

191 2012). A precise comparison on the EoS of KCl between Dewaele et al. (2012) and ours
192 may be made using the curve from Dorogokupets and Oganov (2007)'s Pt scale in Fig. 6a,
193 as Dewaele et al. (2012) used the ruby scale proposed by Dorogokupets and Oganov
194 (2007). The comparison indicates that our EoS gives a lower pressure at a given volume
195 of KCl. In other words, our compression curve gives a smaller volume at a given pressure,
196 which may arise due to the different stress state developed in the sample chamber.
197 Dewaele et al. (2012) used a single crystal of KCl loaded in He. Helium is known to be a
198 good pressure-transmitting medium even after solidification above 10 GPa. As we
199 discussed above, our P - V - T data represent lesser nonhydrostatic conditions than
200 experiments with a He pressure medium without thermal annealing (Dorfman et al. 2012).
201 Also, Takamura and Dewaele (2008) reported the stress state of gold loaded in He
202 medium, and argued that the deviation from the hydrostatic condition becomes prominent
203 under high pressure, particularly at Mbar pressures.

204 **Thermal equation of state**

205 To construct a thermal EoS for B2 KCl, all the high-temperature data were
206 analyzed in the framework of a thermal pressure EoS. At a constant sample volume, the
207 following equation holds

$$208 \quad P(V, T) = P(V, T_0) + \Delta P_{th} \quad (2)$$

209 where ΔP_{th} is the thermal pressure term. We evaluated the thermal pressure term based
210 on the Mie–Grüneisen–Debye model (e.g., Jackson and Rigden 1996)

$$211 \quad \Delta P_{th} = \frac{\gamma}{V} [E_{th}(V, T) - E_{th}(V, T_0)] \quad (3)$$

212 where γ and E_{th} are the Grüneisen parameter and internal thermal energy, respectively.

213 The thermal energy is calculated from the Debye approximation

$$214 \quad E_{th} = \frac{9nRT}{(\theta/T)^3} \int_0^{\theta/T} \frac{x^3}{e^x - 1} dx \quad (4)$$

215 where n and R , and θ are the number of atoms per formula unit, gas constant, and Debye

216 temperature, respectively. The volume dependence of Grüneisen parameter (q) is

217 expressed as

$$218 \quad \gamma(V) = \gamma_0 \left(\frac{V}{V_0}\right)^q \quad (5)$$

$$219 \quad \theta = \theta_0 \exp\{[\gamma_0 - \gamma(V)]/q\} \quad (6)$$

220 where θ_0 and γ_0 are the Debye temperature and Grüneisen parameter at ambient

221 condition, respectively. Fitting all the high temperature data simultaneously yielded $\gamma_0 =$

222 0.58 ± 0.05 and $q = 0.9 \pm 0.2$ with θ_0 fixed at 235 K (Gray 1963). Calculated isothermal

223 compression curves from this model and the P - V - T data are presented in Figure 4b. We

224 also evaluated the EoS based on Holmes et al. (1989)'s Pt scale (Table 2). The obtained

225 Grüneisen parameter is again as small as 0.46 ± 0.05 with $q = 0.7 \pm 0.3$. The fitted

226 parameters are listed in Table 2.

227 Another thermal pressure EoS, which is known as the thermodynamic thermal

228 pressure model (Jackson and Rigden 1996), was also employed. In this EoS, instead of

229 Eq. (3), the following equation is applied

$$230 \quad \Delta P_{th} = \int_{T_0}^T [\alpha K_T]_V dT \cong \alpha K_T (T - T_0) \quad (7)$$

231 where α is the volumetric thermal expansivity, and K_T is the isothermal bulk modulus.
232 Here αK_T was assumed to be a constant, which is reasonable when the temperature range
233 is much higher than the Debye temperature (235 K for KCl). The fitting of all the data
234 yielded $\alpha K_T = 0.0037 \pm 0.0001$ GPa/K. We also found a similar value of $\alpha K_T = 0.0033$
235 ± 0.0002 GPa/K when Holmes et al. (1989)'s Pt scale was used.

236 Both of the two different Pt scales yielded the very low thermal expansivity of B2
237 KCl. The αK_T term in this study was found to be higher than that obtained based on
238 theoretical calculations (0.00224 GPa/K) and experiments up to 8 GPa (0.00284 GPa/K)
239 (Walker et al. 2002; Dewaele et al. 2012) (Table 2). Note that the thermal expansivity of
240 B2 KCl is still low compared with B2 NaCl. A DAC experiment on B2 NaCl reported a
241 larger Grüneisen parameter $\gamma_0 = 1.70$ (Fei et al. 2007), which corresponds to $\alpha K_T =$
242 0.0040 GPa/K. Theoretical calculations also reported small αK_T of B2 NaCl ranging
243 from 0.00328 to 0.00468 GPa/K (Ueda et al. 2008; Ono et al. 2010). Figure 6b shows
244 thermal pressures of B2 KCl calculated from the Mie–Grüneisen–Debye model in this
245 study. The calculated thermal pressure is almost pressure insensitive due to the small
246 Grüneisen parameter. This is in good agreement with Dewaele et al. (2012), in which the
247 thermal pressure is assumed to be independent of volume.

248 **IMPLICATIONS**

249 In order to determine the accurate sample pressure at a high temperature in a
250 laser-heated DAC experiment, pressure calibrants such as Pt, Au, and MgO are
251 commonly mixed with the sample so that both materials are under the identical

252 temperature condition. However, for a study of the Earth's core materials (pure iron or its
253 alloy with light elements), this is not suitable due to the potential chemical reactions. A
254 KCl would be an alternative high-*T* pressure calibrant. The present study revealed that
255 KCl shows a small thermal pressure at any given pressure. For instance, the thermal
256 pressure of KCl is as small as ~10 GPa at 3000 K, then increases to ~15 GPa at 4000 K
257 regardless of the pressure, which are ~40% smaller than the case for Pt, Au, or MgO
258 (Tange et al. 2009; Yokoo et al. 2009). Such low thermal expansivity allows for
259 calculating the sample pressure on heating from the EOS of B2 KCl as a pressure
260 medium even in the case of the large temperature gradients present within KCl layers.
261 The temperature of the KCl pressure medium may be corrected downward from the
262 measured sample temperature to account for axial thermal gradients through the
263 insulating layer (Campbell et al. 2009), which will reduce the pressure uncertainty to as
264 small as a few GPa. In conclusion, the determined low thermal pressure of B2 KCl
265 validates the use of a KCl medium as a high-*T* pressure marker. This would add another
266 advantage of KCl over the other materials to the soft and chemically inert natures.

267 **ACKNOWLEDGMENTS**

268 Yoichi Nakajima is acknowledged for fruitful discussion about equation of state.
269 We also thank Haruka Ozawa for her technical assistance. Comments from an
270 anonymous reviewer were helpful to improve the manuscript. The synchrotron X-ray
271 diffraction experiments were performed at BL10XU, SPring-8 (proposal Nos.
272 2012A0087, 2012B0087 and 2013B0087). TK was supported by the European Research
273 Council (ERC) Consolidator Grant (#647723).

274

275

REFERENCES CITED

276

277 Andrault, D., Pesce, G., Bouhifd, M.A., Bolfan-Casanova, N., Hénot, J.-M., and

278 Mezouar, M. (2014) Melting of subducted basalt at the core–mantle boundary.

279 Science, 344, 892–895.

280 Anzellini, S., Dewaele, A., Mezouar, M., Loubeyre, P., and Morard, G. (2013) Melting of

281 iron at Earth’s inner core boundary based on fast X-ray diffraction. Science, 340,

282 464–466.

283 Boehler, R., Ross, M., and Boercker, D.B. (1997) Melting of LiF and NaCl to 1 Mbar:

284 Systematics of ionic solids at extreme conditions. Physical Review Letters, 78,

285 4589–4592.

286 Campbell, A.J. and Heinz, D.L. (1991) Compression of KCl in the B2 structure to 56 GPa.

287 Journal of Physics and Chemistry of Solids, 52, 495–499.

288 Campbell, A.J., Danielson, L., Righter, K., Seagle, C.T., Wang, Y., and Prakapenka, V.B.

289 (2009) High pressure effects on the iron–iron oxide and nickel–nickel oxide oxygen

290 fugacity buffers. Earth and Planetary Science Letters, 286, 556–564.

291 Dewaele, A., Belonoshko, A.B., Garbarino, G., Ocelli, F., Bouvier, P., Hanfland, M., and

292 Mezouar, M. (2012) High-pressure-high-temperature equation of state of KCl and

293 KBr. Physical Review B, 85, 214105.

294 Dorfman, S M., Prakapenka, V. B., Meng, Y., and Duffy, T.S. (2012) Intercomparison of

295 pressure standards (Au, Pt, Mo, MgO, NaCl and Ne) to 2.5 Mbar, Journal of

296 Geophysical Research, 117, B08210.

- 297 Dorogokupets, P.I., and Oganov, A.R. (2007) Ruby, metals, and MgO as alternative
298 pressure scales: A semiempirical description of shock-wave, ultrasonic, X-ray, and
299 thermochemical data at high temperatures and pressures. *Physical Review B*, 75,
300 024115.
- 301 Fei, Y., Ricolleau, A., Frank, M., Mibe, K., Shen, G., and Prakapenka, V.B. (2007)
302 Toward an internally consistent pressure scale, *Proceedings of the National*
303 *Academy of Sciences of the United States of America*, 104, 9182–9186.
- 304 Gray, D.E. (1963) *American Institute of Physics Handbook*, 2nd ed. (McGraw-Hill, New
305 York).
- 306 Holmes, N.C., Moriarty, J.A., Gathers, G.R., and Nellis, W.J. (1989) Equations of state of
307 platinum to 660 GPa (6.6 Mbar). *Journal of Applied Physics*, 66, 2962–2967.
- 308 Jackson, I. and Rigden, S.M. (1996) Analysis of P-V-T data: Constraints on the
309 thermoelastic properties of high-pressure minerals. *Physics of the Earth and*
310 *Planetary Interiors*, 96, 85–112.
- 311 Komabayashi, T., Hirose, K., Ohishi, Y. (2012) In situ X-ray diffraction measurements of
312 the fcc–hcp phase transition boundary of an Fe–Ni alloy in an internally heated
313 diamond anvil cell. *Physics and Chemistry of Minerals*, 39, 329–338.
- 314 Menéndez-Proupin, E., and Singh, A.K. (2007) *Ab initio* calculations of elastic properties
315 of compressed Pt. *Physical Review B*, 76, 054117.
- 316 Morard, G., Andrault, D., Antonangeli, D., Nakajima, Y., Auzende, A.L., Boulard, E.,
317 Cervera, S., Clark, A., Lord, O.T., Siebert, J., Svitlyk, V., Garbarino, G., and
318 Mezouar, M. (2017) Fe–FeO and Fe–Fe₃C melting relations at Earth's core–mantle
319 boundary conditions: Implications for a volatile-rich or oxygen-rich core, *Earth and*

- 320 Planetary Science Letters, 473, 94–103.
- 321 Ohishi, Y., Hirao, N., Sata, N., Hirose, K., and Takata, M. (2008) Highly intense
322 monochromatic X-ray diffraction facility for high-pressure research at SPring-8.
323 High Pressure Research, 28, 163–173.
- 324 Ono, S. (2010) The equation of state of B2-type NaCl, Journal of Physics: Conference
325 Series, 215, 012196.
- 326 Ono, S., Brodholt, J.P., and Price, G.D. (2011) Elastic, thermal and structural properties
327 of platinum. Journal of Physics and Chemistry of Solids, 72, 169–175.
- 328 Sakai, T., Ohtani, E., Hirao, N., and Ohishi, Y. (2011) Equation of state of the NaCl-B2
329 phase up to 304 GPa, Journal of Applied Physics, 109, 084912.
- 330 Seto, Y., Nishio-Hamane, D., Nagai, T., Sata, N. (2010) Development of a software suite
331 on X-ray diffraction experiments. The Review of High Pressure Science and
332 Technology, 20, 269–276.
- 333 Shim, S-H., Duffy, T.S., and Shen, G. (2000) The equation of state of CaSiO₃ perovskite
334 to 108 GPa at 300 K. Physics of the Earth and Planetary Interiors, 120, 327–338.
- 335 Singh, A.K. (2009) Analysis of nonhydrostatic high-pressure diffraction data (cubic
336 system): Assessment of various assumptions in the theory, Journal of Applied
337 Physics, 106, 043514.
- 338 Singh, A.K., and Takemura, K. (2001) Measurement and analysis of nonhydrostatic
339 lattice strain component in niobium to 145 GPa under various fluid pressure-
340 transmitting media, Journal of Applied Physics, 90, 3269.
- 341 Singh, A. K., H. Liermann, Y. Akahama, S. K. Saxena, and E. Menéndez-Proupin (2008),
342 Strength of polycrystalline coarse-grained platinum to 330 GPa and of

- 343 nanocrystalline platinum to 70 GPa from high-pressure X-ray diffraction data,
344 Journal of Applied Physics, 103, 063524.
- 345 Sokolova, T.S., Dorogokupets, P.I., Dymshits, A.M., Danilov, B.S., and Litasov, K.D.
346 (2016) Microsoft excel spreadsheets for calculation of P – V – T relations and
347 thermodynamic properties from equations of states of MgO, diamond and nine
348 metals as pressure markers in high-pressure and high-temperature experiments,
349 Computers and Geosciences, 94, 162–169.
- 350 Takemura, K., and Dewaele, A. (2008) Isothermal equation of state for gold with a He-
351 pressure medium, Physical Review B, 78, 104119.
- 352 Tange, Y., Y. Nishihara, and T. Tsuchiya (2009), Unified analyses for P – V – T equation of
353 state of MgO: A solution for pressure-scale problems in high P – T experiments,
354 Journal of Geophysical Research, 114, B03208.
- 355 Tateno, S., Kuwayama, Y., Hirose, K., and Ohishi, Y. (2015) The structure of Fe–Si alloy
356 in Earth’s inner core. Earth and Planetary Science Letters, 418, 11–19.
- 357 Ueda, Y., Matsui, M., Yokoyama, A., Tange, Y., and Funakoshi K. (2008) Temperature-
358 pressure-volume equation of state of the B2 phase of sodium chloride, Journal of
359 Applied Physics, 103, 113513.
- 360 Uts, I., Glazyrin, K., and Lee, K.K.M. (2013) Effect of laser annealing of pressure
361 gradients in a diamond-anvil cell using common solid pressure media, Review of
362 Scientific Instrument, 84, 103904.
- 363 Walker, D., Cranswick, L.M.D., Verma, P.K., Clark, S.M., and Buhre, S. (2002) Thermal
364 equation of state for B1 and B2 KCl, American Mineralogist, 87, 805–812.
- 365 Yagi, T. (1978) Experimental determination of thermal expansivity of several alkali

366 halides. Journal of Physics and Chemistry of Solids, 39, 563–571.
367 Yokoo, M., Kawai, N., Nakamura, K.G., Kondo, K., Tange, Y., and Tsuchiya, T. (2009)
368 Ultrahigh-pressure scales for gold and platinum at pressures up to 550 GPa, Physical
369 Review B, 80, 104114.

370

371 **Figure captions**

372 **FIGURE 1.** Integrated XRD pattern collected (a) in situ at 1820 K and 22 GPa in run #4,
373 where B2 KCl, Pt (pressure marker), and Ar (pressure medium) are observed. XRD
374 patterns obtained after thermal annealing at (b) 104 GPa and (c) 229 GPa in runs #2 and
375 #1, respectively, are also shown.

376 **FIGURE 2.** The gamma plot at selected pressures for (a) Pt and (b) B2 phase of KCl
377 before and after thermal annealing shown in blue and red, respectively (see the text for
378 details). The variation of lattice parameters is indicated for different (*hkl*), where $a_m(hkl)$
379 is the measured lattice parameter calculated from individual (*hkl*), and a is the mean
380 lattice parameter calculated from all reflections. The solid line is a least-squares fit to the
381 data. According to current analysis, $a_m(200)$ and $a_m(400)$ for Pt and $a_m(200)$ for B2 KCl
382 are not used for calculating unit-cell volume.

383 **FIGURE 3.** Differential stress, t , and St value measured in (a) Pt and (b) B2 KCl,
384 respectively, before (blue) and after (red) thermal annealing. Previous measurements of t
385 values in Pt loaded in He pressure medium are also shown (gray) (Dorfman et al. 2012).
386 Nonhydrostatic effect is clearly reduced after laser heating. The St values of KCl before
387 heating at $P > 200$ GPa are greater than $|0.1|$ and beyond the range of the diagram.

388 **FIGURE 4.** Variation of full width at half maximum (FWHM) normalized to diffraction
389 angle ($\Delta(2\theta)/(2\theta)$) of the most intense reflection from (111) and (110) of (a) Pt and (b) B2
390 KCl, respectively. Peak width before heating (blue) is reduced by laser annealing (red).
391 Cold compression data for Pt in He medium also shown (gray) (Dorfman et al. 2012).
392 Shadow indicates the range of FWHM of the diffraction peaks from (111) to (422) of
393 CeO₂ standard as a reference.

394 **FIGURE 5.** (a) Volume data for B2 KCl and fit to the Vinet EoS at room temperature.
395 Pressures are calculated from the EoS of Pt proposed by Sokolova et al. (2016). All data
396 are collected after laser annealing. Broken line denotes previous cold compression data
397 with He pressure medium (Dewaele et al. 2012). (b) Volume data for 300 K and high-
398 temperature and isothermal compression curve based on the Mie–Grüneisen–Debye
399 model.

400 **FIGURE 6.** (a) The comparison with our EoS based on various pressure scales and that
401 obtained in Dewaele et al. (2012) calibrated by ruby pressure gauge by Dorogokupets and
402 Oganov, 2007, which is consistent with their Pt scale. (b) Thermal pressures at different
403 temperatures calculated from present study based on the Mie–Grüneisen–Debye model
404 (solid line) and those from Dewaele et al. (2012) based on simple linear temperature
405 dependence independent from volume (broken line).

TABLE 1. Unit-cell parameters of Pt and B2 KCl

Run	P (GPa) ^a	\pm	T (K)	\pm	Pt			
					a (Å)	\pm	V (Å ³)	\pm
#1	126.2	0.3	300		3.6188	0.0004	47.39	0.01
	143.7	1.3	300		3.5950	0.0017	46.46	0.07
	163.5	2.1	300		3.5704	0.0025	45.52	0.10
	189.3	1.1	300		3.5413	0.0012	44.41	0.04
	201.9	2.0	300		3.5282	0.0020	43.92	0.07
	212.2	2.2	300		3.5178	0.0022	43.53	0.08
	228.6	2.0	300		3.5021	0.0018	42.95	0.07
#2	84.8	0.3	300		3.6853	0.0006	50.05	0.02
	103.7	0.5	300		3.6528	0.0008	48.74	0.03
	119.0	0.4	300		3.6293	0.0005	47.80	0.02
#3	10.0	0.2	1640	10	3.8964	0.0003	59.16	0.01
	10.2	0.3	1780	10	3.8839	0.0005	58.59	0.02
	9.7	0.3	1480	10	3.8488	0.0004	57.01	0.02
	6.0	0.1	300		3.8097	0.0010	55.29	0.04
	14.1	0.3	2080	10	3.9040	0.0002	59.50	0.01
	9.0	0.1	300		3.9019	0.0001	59.40	0.01
	22.8	0.4	2160	30	3.8373	0.0004	56.51	0.02
	20.7	0.1	1490	10	3.8240	0.0006	55.92	0.03
	18.4	0.1	300		3.7870	0.0007	54.31	0.03
	31.6	0.5	2390	60	3.7652	0.0007	53.38	0.03
	30.1	0.1	1780	20	3.7470	0.0004	52.61	0.02
	37.0	0.2	2560	10	3.9246	0.0005	60.45	0.02
	30.6	0.3	300		3.9289	0.0003	60.65	0.01
	48.3	0.3	2390	30	3.9199	0.0005	60.23	0.02
46.6	0.7	1790	10	3.9208	0.0005	60.27	0.02	
#4	4.2	0.1	300		3.8844	0.0008	58.61	0.03
	8.7	0.9	1680	100	3.8728	0.0005	58.09	0.02
	4.7	0.0	300		3.8573	0.0005	57.39	0.02
	22.2	0.9	1820	110	3.8462	0.0003	56.90	0.01
	27.2	0.2	1890	20	3.8425	0.0012	56.73	0.05
	21.8	0.1	300		3.8028	0.0004	55.00	0.02
	31.0	0.6	1990	50	3.7950	0.0009	54.66	0.04
	25.9	0.2	300		3.9324	0.0008	60.81	0.04
	38.7	0.3	300		3.8766	0.0004	58.26	0.02

47.1	0.3	300		3.8597	0.0002	57.50	0.01
60.7	2.5	2210	210	3.8487	0.0007	57.01	0.03
58.1	1.8	1640	170	3.7660	0.0023	53.41	0.10
59.4	0.8	2300	200	3.7620	0.0013	53.24	0.05
54.7	0.2	300		3.7710	0.0019	53.63	0.08

^aPressure was calculated based on the equation of state proposed by Sokolova et al. (2016).

^b*t* values at high temperature are calculated with elastic anisotropy factor at 300 K for refer

B2 KCl							
t (GPa) ^b	\pm	a (Å)	\pm	V (Å ³)	\pm	St	\pm
0.92	0.32	2.8682	0.0039	23.5946	0.0957	0.0021	0.0130
0.35	0.97	2.8256	0.0014	22.5587	0.0329	0.0068	0.0029
1.82	1.49	2.7919	0.0040	21.7624	0.0946	0.0072	0.0056
0.85	1.81	2.7522	0.0027	20.8474	0.0625	0.0060	0.0021
1.40	-	2.7346	0.0009	20.4485	0.0210	-0.0114	-
0.48	1.56	2.7217	0.0004	20.1622	0.0086	0.0127	-
0.68	0.13	2.6997	0.0004	19.6761	0.0094	0.0129	-
1.00	0.26	2.9757	0.0011	26.3493	0.0297	0.0030	0.0020
0.97	0.19	2.9187	0.0005	24.8627	0.0137	0.0035	0.0010
0.81	0.43	2.8829	0.0012	23.9597	0.0300	0.0081	0.0025
0.06	0.10	3.5581	0.0008	45.0463	0.0321	0.0058	0.0026
0.14	0.11	3.4902	0.0012	42.5142	0.0428	-0.0019	0.0050
0.03	0.13	3.3543	0.0018	37.7402	0.0592	-0.0019	0.0021
0.11	0.07	3.2359	0.0016	33.8821	0.0500	-0.0018	0.0013
0.17	0.15	3.6194	0.0005	47.4154	0.0183	0.0003	0.0001
0.00	0.13	3.5984	0.0000	46.6154	0.0017	0.0011	0.0016
0.29	0.21	3.3148	0.0013	36.4220	0.0431	0.0005	0.0006
-0.11	0.08	3.2753	0.0006	35.1356	0.0183	0.0014	0.0006
0.23	0.15	3.1833	0.0018	32.2575	0.0537	-0.0021	0.0023
0.01	0.10	3.1321	0.0005	30.7265	0.0146	-0.0004	0.0011
-0.15	0.05	3.0934	0.0004	29.6002	0.0103	0.0016	0.0019
0.23	0.24	3.5717	0.0020	45.5635	0.0769	0.0004	0.0004
0.02	0.29	3.5795	0.0036	45.8620	0.1389	-0.0010	0.0028
-0.13	0.08	3.5790	0.0014	45.8456	0.0542	-0.0001	0.0007
0.17	0.41	3.5062	0.0001	43.1025	0.0035	0.0006	0.0007
0.02	0.07	3.3718	0.0004	38.3338	0.0134	0.0007	0.0009
-0.06	0.17	3.3701	0.0004	38.2765	0.0125	0.0016	0.0022
0.04	0.03	3.2952	0.0009	35.7800	0.0283	-0.0024	0.0011
-0.11	0.06	3.2905	0.0015	35.6260	0.0472	-0.0001	0.0023
-0.02	0.06	3.2497	0.0004	34.3199	0.0133	0.0024	0.0018
0.00	0.13	3.1633	0.0004	31.6537	0.0127	-0.0016	0.0016
-0.13	0.17	3.1618	0.0002	31.6079	0.0063	0.0004	0.0002
0.09	0.12	3.5952	0.0004	46.4679	0.0151	-0.0030	0.0007
0.33	0.49	3.3820	0.0013	38.6842	0.0442	-0.0004	0.0022

0.30	0.17	3.3260	0.0003	36.7925	0.0105	0.0019	0.0018
0.70	0.70	3.2870	0.0002	35.5151	0.0060	0.0024	0.0005
-0.20	0.40	3.1000	0.0008	29.7923	0.0235	0.0029	0.0014
-0.09	0.61	3.0983	0.0012	29.7421	0.0332	0.0041	0.0022
-0.27	0.13	3.0994	0.0019	29.7747	0.0539	-0.0003	0.0006

ence.

TABLE 2. Thermoelastic parameters for B2 KCl

	V_0^* (\AA^3)	K_0 (GPa)	\pm	K'_0	\pm	γ_0	\pm	q	\pm
This study	<i>Sokolova's Pt scale</i>								
	54.5	18.3	0.3	5.60	0.03	0.58	0.05	0.9	0.2
	54.5	18.3	0.2	5.60	0.03				
	<i>Holmes' Pt scale</i>								
	54.5	17.4	0.2	5.77	0.04	0.46	0.05	0.7	0.3
	54.5	17.7	0.3	5.60	0.04				
Dewaele et al. (2012)	54.5	17.2		5.89					
Walker et al. (2002)	53.53	23.7		4.4					
Campbell & Heinz (1991)	53.8	24.6		5.2					

Note: V_0 is fixed during fitting to 54.5 (\AA^3) from Dewaele et al. (2012).

αK	\pm	α
(GPa/K)		(1/K)
0.0037	0.0001	
0.0033	0.0002	
0.00224		
0.00284		0.00012

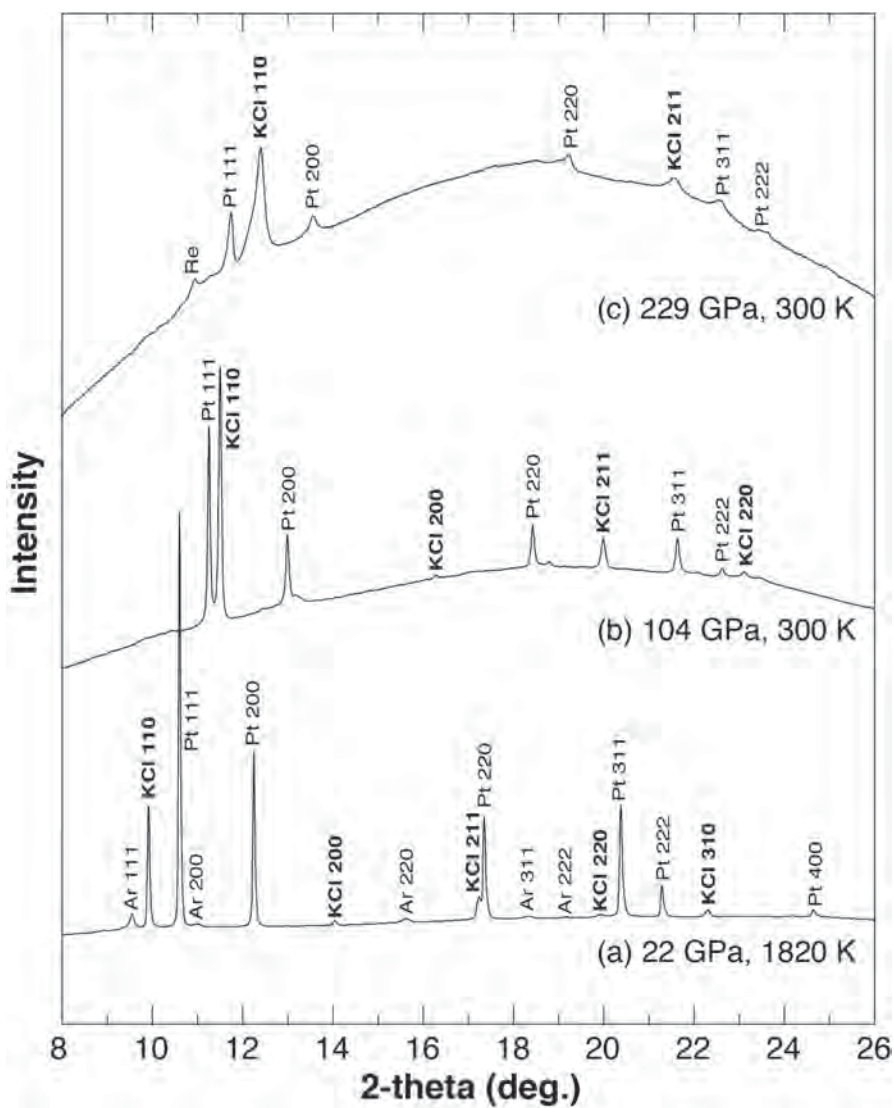


Fig. 1

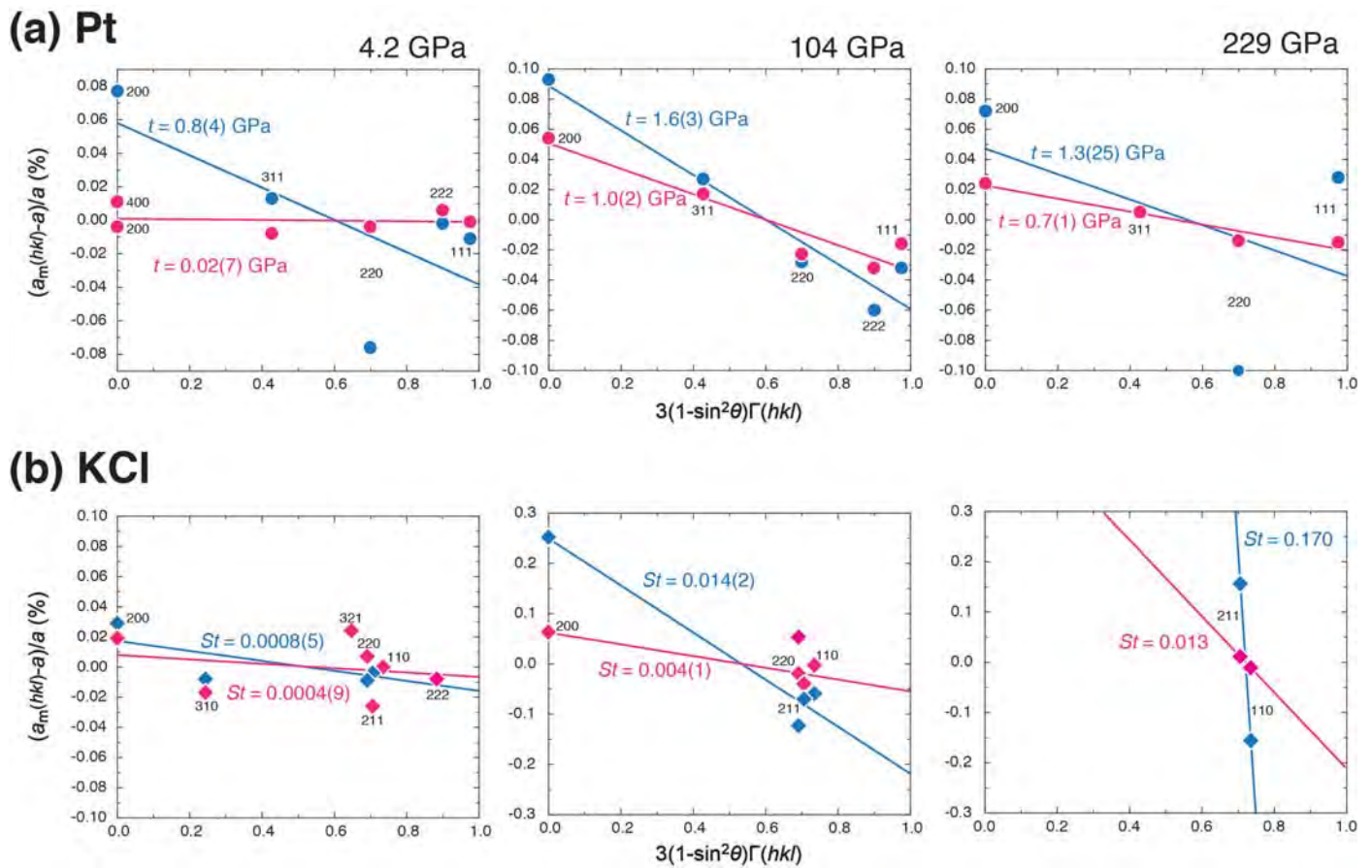


Fig. 2

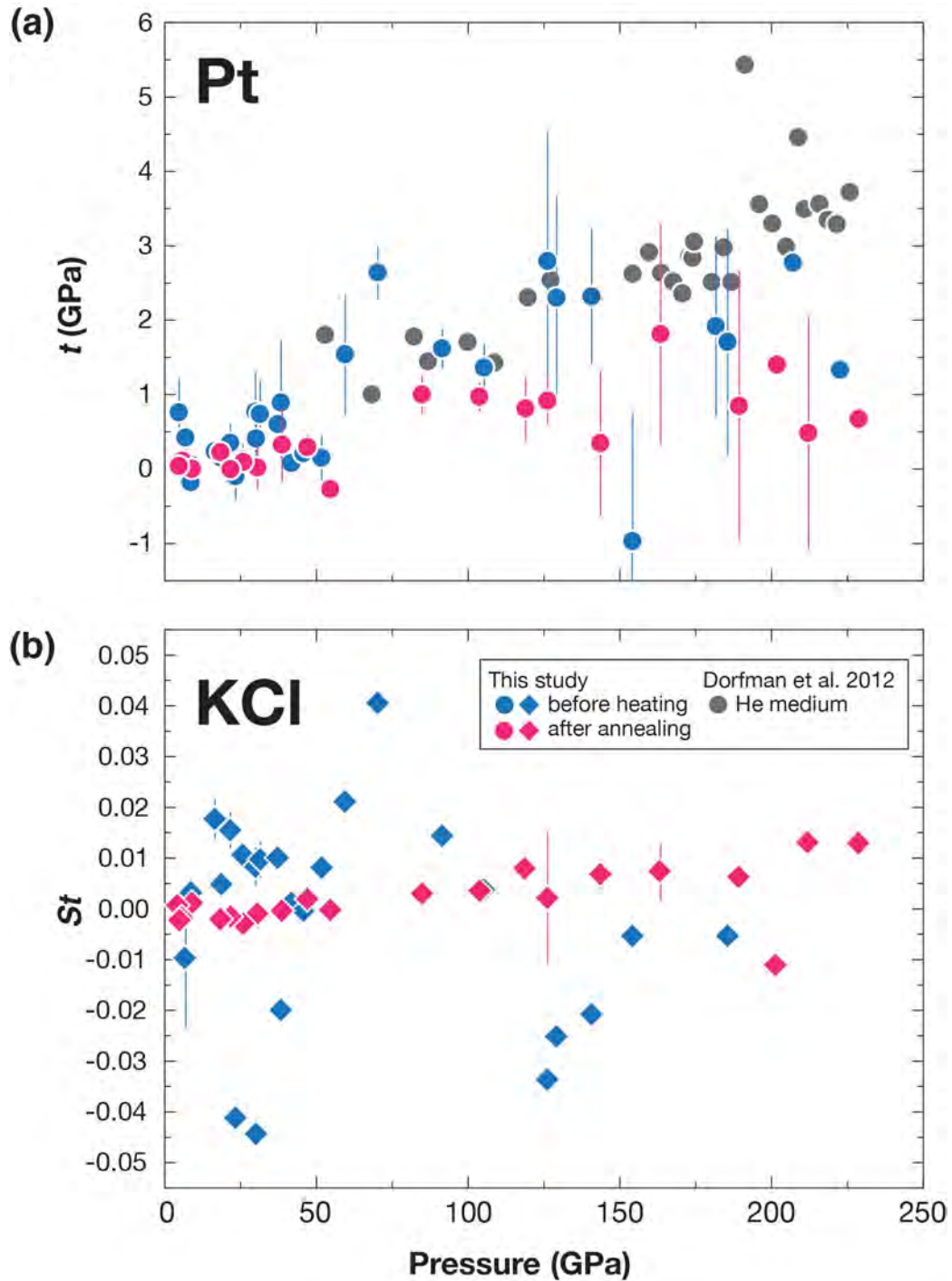


Fig. 3

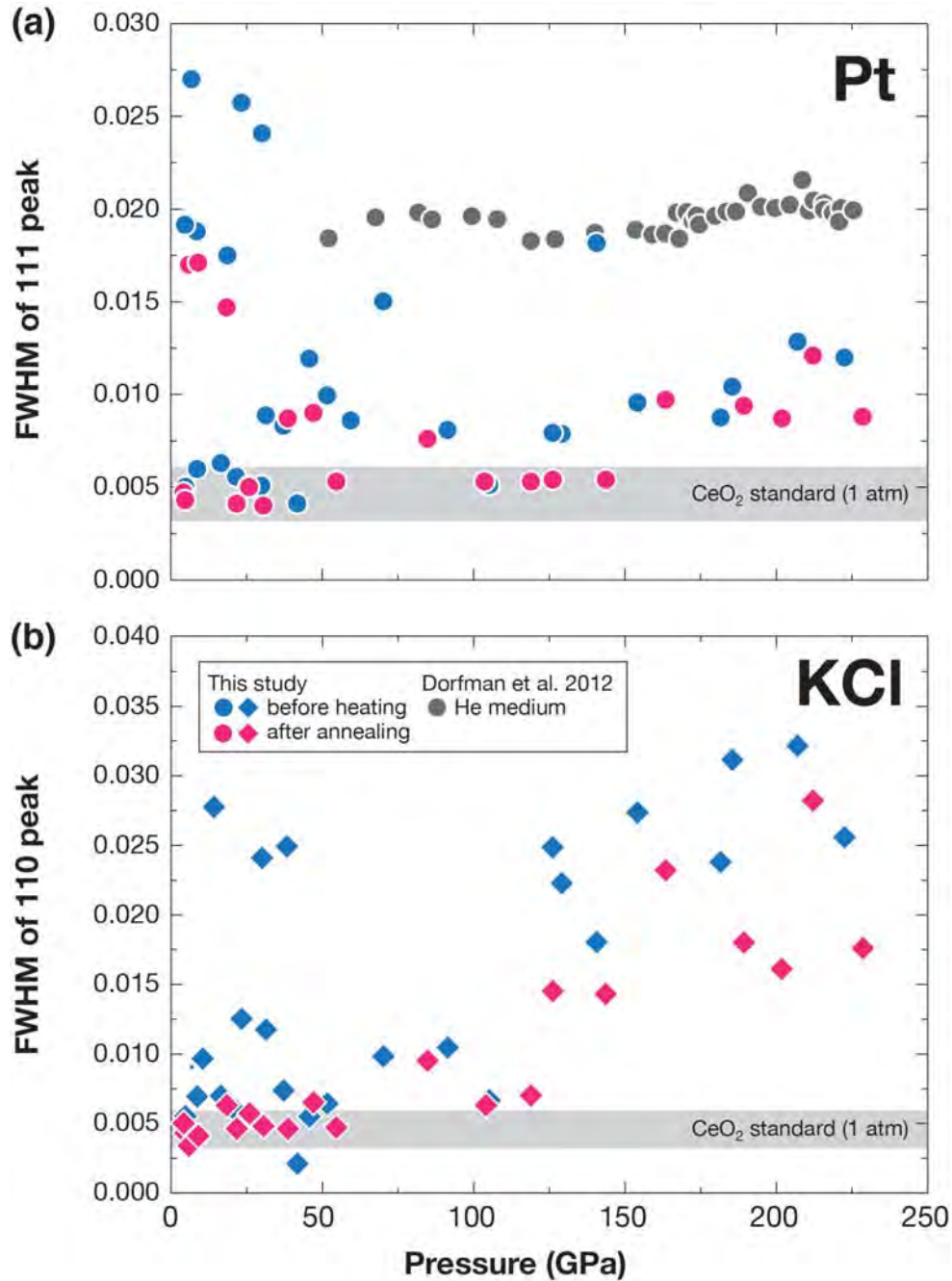


Fig. 4

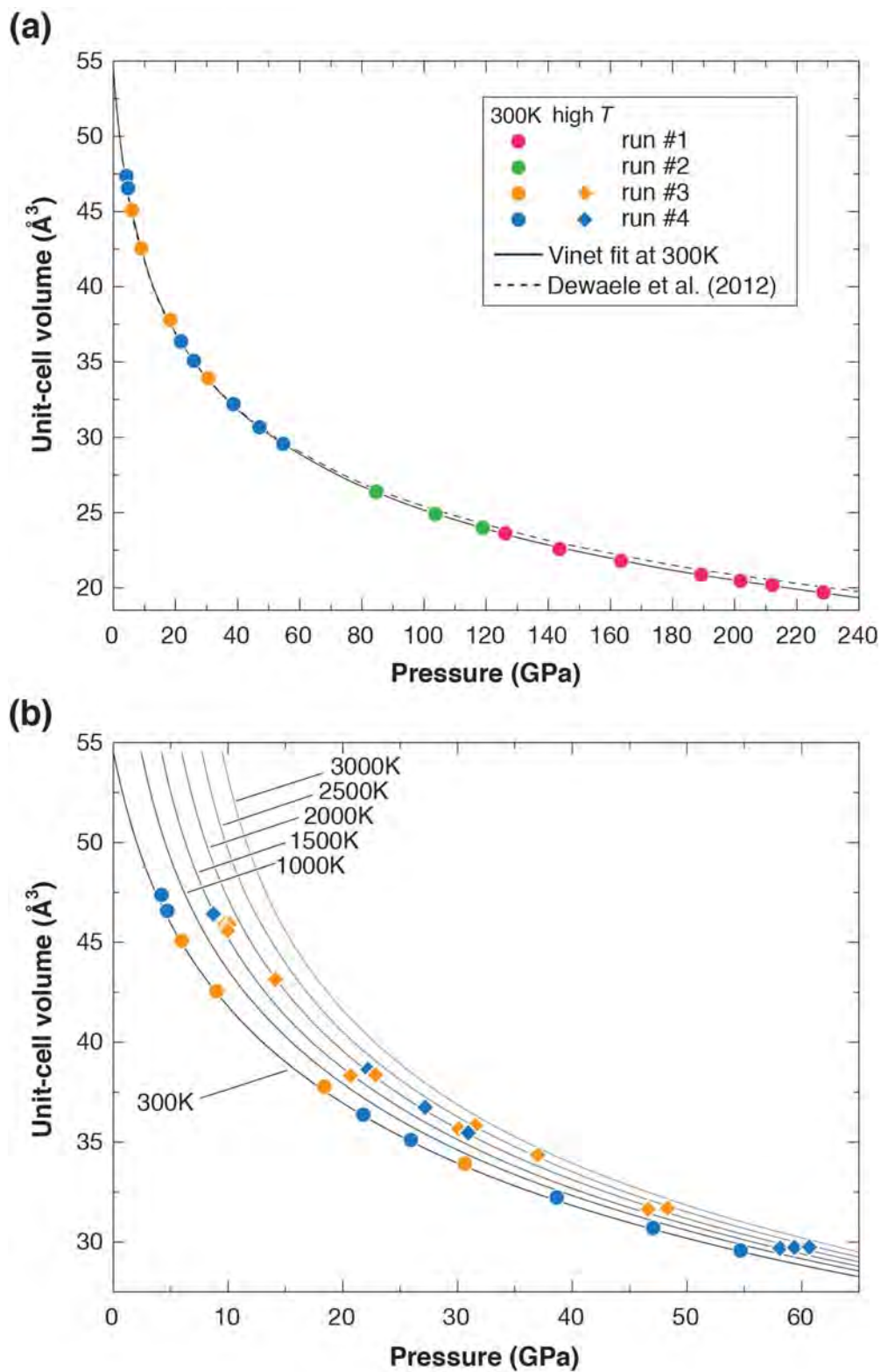


Fig. 5

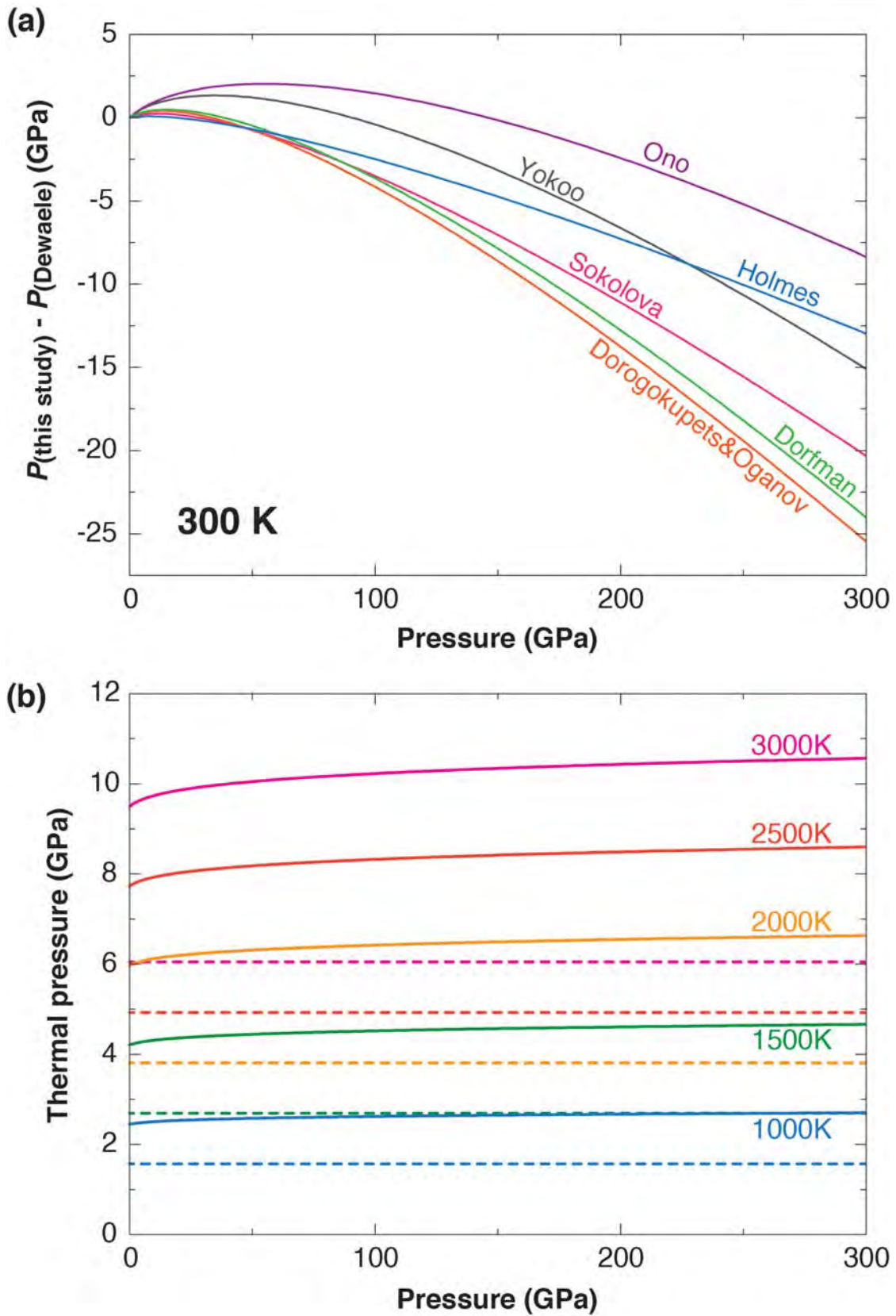


Fig. 6